

# Purported quantitative support for multiple introductions of SARS-CoV-2 into humans is an artefact of an imbalanced hypothesis testing framework

Angus McCowan\*

## Abstract

A prominent report claimed substantial support for two introductions of SARS-CoV-2 into humans using a calculation that combined phylodynamic inferences and epidemic models. Inspection of the calculation identifies an imbalance in the hypothesis testing framework that confounds this result; the single-introduction model was tested against more stringent conditions than the two-introduction model. Here, I show that when the two-introduction model is tested against the same conditions, the support disappears.

Understanding the number of SARS-CoV-2 introductions into humans is useful for estimating the genetic diversity in the source, and is also relevant to understanding possible links between the source and particular infection clusters.

A prominent report [1] reviewed genomic data from early in the epidemic and concluded that sequences outside of two main clades were unreliable. The authors then hypothesized that the two clades arose from separate introductions into humans, and quantified support for this hypothesis with a Bayes factor (BF) that compared the plausibility of their curated genomic data ( $\mathbf{Y}$ ) arising from two successful introductions ( $I_2$ ) versus one ( $I_1$ ),

$$\text{BF} = \frac{P(\mathbf{Y}|I_2)}{P(\mathbf{Y}|I_1)}. \quad (1)$$

The published Bayes factor was 60, with which the authors claimed strong support for multiple introductions. Subsequent replication efforts identified three errors in the calculation: a syntax error caused undercounting of one-introduction likelihoods; an erroneous normalization disproportionately inflated the two-introduction likelihoods; and non-exclusive marginalization caused double-counting of two-introduction likelihoods. With a subsequent erratum [2], the syntax error was corrected, the erroneous normalization removed and the marginalization made exclusive. As a result, the Bayes factor dropped to 4.

---

\*awmccowan@fastmail.com

A Bayes factor of 4 should normally indicate substantial or moderate support. However, there is an imbalance in the conditioning of the likelihoods used to calculate Equation 1.

The imbalance is the focus of this investigation. I do not attempt to address issues with data, modelling, assumptions or the conditions themselves. Instead, I identify the imbalance in the conditioning of the likelihoods and explore its effect on the Bayes factor using a simple model. I also evaluate its effect on the Bayes factor replicating the authors' assumptions. I then briefly discuss the significance and set out the methods I used in detail.

## Identifying the imbalance

The authors marginalized the Bayes factor 1 over ancestral haplotypes ( $S_{\text{MRCA}}$ ) and virus tree topologies ( $\tau$ ), while assuming equal prior probabilities for ancestral haplotypes to derive

$$\text{BF} = \frac{\sum_{S_{\text{MRCA}}} P(S_{\text{MRCA}}|\mathbf{Y}) \left[ \sum_{\tau} P(S_{\text{MRCA}}|\tau) P(\tau|I_2) \right]}{\sum_{S_{\text{MRCA}}} P(S_{\text{MRCA}}|\mathbf{Y}) \left[ \sum_{\tau} P(S_{\text{MRCA}}|\tau) P(\tau|I_1) \right]} \quad (2)$$

where

$$P(S_{\text{MRCA}}|\tau) \propto \begin{cases} 1 & \text{if } \tau \text{ and } S_{\text{MRCA}} \text{ are compatible} \\ 0 & \text{otherwise} \end{cases} \quad (3)$$

and

$$\sum_{S_{\text{MRCA}}} P(S_{\text{MRCA}}|\tau) = 1 \quad \text{for all } \tau. \quad (4)$$

That is, the Bayes factor mixed posterior probabilities ( $P(S_{\text{MRCA}}|\mathbf{Y})$ ) with likelihoods ( $P(\tau|I)$ ) through compatibility equations ( $P(S_{\text{MRCA}}|\tau)$ ), such that each likelihood was weighted according to the average posterior probability of the ancestral haplotypes compatible with that topology.

The authors inferred the posterior probabilities,  $P(S_{\text{MRCA}}|\mathbf{Y})$ , using Bayesian phylodynamic inference, and identified four candidates for the ancestral haplotype:  $S_A$  (the root of the clade closest to bat viruses),  $S_B$  (the root of the other main clade, differing from  $S_A$  by two mutations),  $S_C$  (differing from  $S_A$  by one of  $S_B$ 's mutations), and  $S_T$  (differing from  $S_A$  by the other of  $S_B$ 's mutations). Under the most plausible inference scheme, which used a synthetic recombinant ancestor (recCA) as root, the authors reported posterior probabilities of  $P(S_A|\mathbf{Y}) = 77\%$ ,  $P(S_B|\mathbf{Y}) = 8\%$ ,  $P(S_C|\mathbf{Y}) = 10\%$  and  $P(S_T|\mathbf{Y}) = 4\%$ . Note that  $S_A$  was found significantly more credible.

The authors estimated the likelihoods,  $P(\tau|I)$ , by simulating 1,100 virus trees, and counting the proportion with topologies deemed compatible with

the phylodynamic inferences. Two one-introduction topologies were considered,  $\tau_{1C}$  and  $\tau_{2C}$ , while a single two-introduction topology was considered,  $(\tau_p, \tau_p)$ . The authors' estimated likelihoods (with 95% Bayesian credible intervals) were  $P((\tau_p, \tau_p)|I_2) = 22.6(19.9, 25.5)\%$ ,  $P(\tau_{1C}) = 3.1(2.2, 4.3)\%$  and  $P(\tau_{2C}) = 0.0(0.0, 0.3)\%$ .

Based on the phylodynamic inferences, the authors deemed  $(\tau_p, \tau_p)$  compatible with  $\{S_A, S_B, S_C, S_T\}$ ,  $\tau_{1C}$  compatible with  $\{S_A, S_B\}$ , and  $\tau_{2C}$  compatible with  $\{S_C, S_T\}$ . With these compatibility statements, Equations 3 and 4 evaluate to the compatibility equations

$$P(S_{\text{MRCA}}|(\tau_p, \tau_p)) = \begin{cases} \frac{1}{4}, & \text{if } S_{\text{MRCA}} \in \{S_A, S_B, S_C, S_T\}, \\ 0, & \text{otherwise,} \end{cases} \quad (5)$$

$$P(S_{\text{MRCA}}|\tau_{1C}) = \begin{cases} \frac{1}{2}, & \text{if } S_{\text{MRCA}} \in \{S_A, S_B\}, \\ 0, & \text{otherwise, and} \end{cases} \quad (6)$$

$$P(S_{\text{MRCA}}|\tau_{2C}) = \begin{cases} \frac{1}{2}, & \text{if } S_{\text{MRCA}} \in \{S_C, S_T\}, \\ 0, & \text{otherwise.} \end{cases} \quad (7)$$

The imbalance lies in the conditioning of the likelihoods,  $P(\tau|I)$ , through the different requirements imposed on the different topologies,  $\tau$ . All topologies were required to have all taxa within only two clades, with a polytomy of at least 100 lineages at the root of each, but the one-introduction topologies were tested against three additional conditions:

- a relative size condition - neither clade could comprise less than 30% of all taxa;
- an evolutionary separation condition - the roots of each clade had to be separated from each other by at least two mutations; and
- a root shape condition - the one-introduction topologies were specified as either  $\tau_{1C}$  (if one of the two clades was ancestral and the other derived), or  $\tau_{2C}$  (if both clades were derived).

One-introduction virus trees that failed to satisfy the relative size and evolutionary separation conditions were excluded from the Bayes factor calculation. Equivalent two-introduction virus trees were not.

One-introduction virus trees were divided by the root shape condition into specific topologies, each with the specific compatibility equations 6 and 7. Two-introduction virus trees were not, but the marginalization gave them the compatibility equation 5, which is the average the one-introduction compatibility equations 6 and 7. This is because of the equal prior probabilities that the authors assigned to ancestral haplotypes. Thus, the compatibility of the one-introduction likelihoods was distributed according by the root shape condition, but that of the two-introduction likelihood was distributed solely by the prior.

The Bayes factor cannot provide meaningful support for the two-introduction hypothesis unless the effect of this imbalance was negligible.

Incidentally, the relative size and evolutionary separation conditions are improper tests for Bayesian analysis in that they test sidedness, rather than agreement. This is potentially a significant source of bias.

Further minor imbalance arises in the filtering of early samples and short-lived lineages. For the one-introduction model, these are determined, respectively, by the first hospitalization and most recent common ancestor (MRCA) of the entire epidemic. For the two-introduction model, these are determined, respectively, by the first hospitalization and MRCA of each clade. Since this filtering involved the human alertness to the epidemic (the start of sampling and detection), the two-introduction filtering should be based on the epidemic, rather than each clade.

## Exploring the effect using a model for introduction diversity

The effect of the imbalance cannot be evaluated directly because the authors' two-introduction model lacks details that would allow the additional conditions to be applied. In particular, the authors do not attempt to model the diversity of the introductions. In order to approximate this diversity, I assume the diversity of each introduction arises with evolution from an MRCA under the molecular clock.

The authors assume each introduction is independent. This means, with the model, that the evolution between the two clades arising from a pair of successful introductions  $(E_x, E_y)$  is affected solely by the times  $(t_x, t_y)$  between the MRCA and each introduction. The independence of each introduction also means that the relative sizes are affected solely through a difference  $|t_x - t_y|$  in the introduction times. Therefore, the ability of any pair of introductions  $(E_x, E_y)$  to satisfy the relative size condition, evolutionary separation condition and root-shape condition is affected solely by the times  $(t_x, t_y)$  between the MRCA and each introduction.

I explore the range of possible times  $(t_x, t_y)$  with the model, to find a conservative the Bayes factor.

In order to accurately estimate the one-introduction likelihoods, I reproduced the authors' epidemic simulations with a hundredfold increase in sample size, to generate 110,000 simulated successful epidemics. Then, following the authors' protocols, I simulated sequencing, coalescence and evolution to generate a virus tree from each successful epidemic, and counted the proportion with topologies  $\tau_{1C}$  and  $\tau_{2C}$ . I did not use the stable coalescent because it would prune short-lived basal lineages, to the benefit of the one-introduction model but not the two-introduction model. The resulting one-introduction likelihoods were  $P(\tau_{1C}|I_1) = 3.1\%$  and  $P(\tau_{2C}|I_1) = 0.1\%$ , matching those reported by the authors.

In order to explore the two-introduction likelihoods, I drew from the 110,000 successful epidemics, with replacement, to obtain 110,000 of pairs  $(E_x, E_y)$  of successful epidemics. I combined each pair  $(E_x, E_y)$  for all timings  $(t_x, t_y) \in \{0, 5, 10, 15, 20, 25, 30\}^2$  days, to obtain 110,000 arrays of 49 combined epidemics. Then, following the authors' protocols, I simulated sequencing, coalescence and evolution to generate a virus tree from each combined epidemic, and counted the proportion with topologies  $\tau_{1C}$  and  $\tau_{2C}$ , where the two clades arose from the separate introductions. I did not use the stable coalescent because in the two-introduction model the basal lineages are successful introductions by definition. The resulting two-introduction likelihoods are shown in Figure 1.

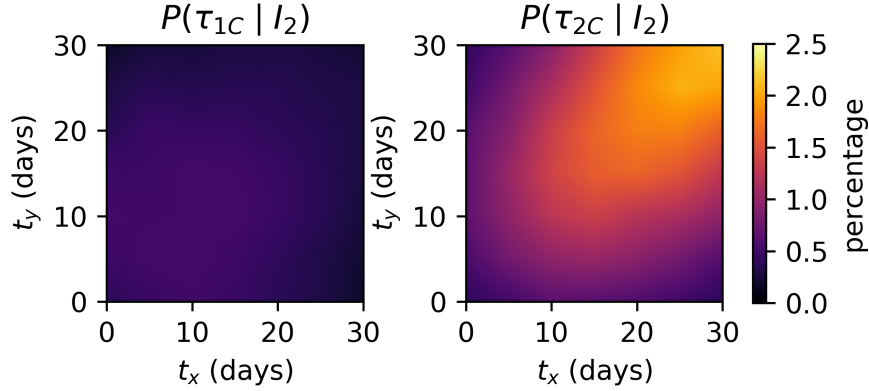


Figure 1: Two-introduction likelihoods for introduction timings  $(t_x, t_y)$

Notably, Figure 1 shows how the conditions combine to place conflicting demands on  $P(\tau_{1C}|I_2)$ . The relative size condition rewards simultaneous introductions, i.e.  $t_x = t_y$ . The evolutionary separation condition rewards a large total time between the MRCA and introductions, i.e.  $(t_x + t_y) \rightarrow \infty$ . In combination, they reward increasing timings along the diagonal  $t_x = t_y$ . This coincidentally reduces the frequency of clades being ancestral and therefore increases the proportion of topologies deemed  $\tau_{2C}$  by the root-shape condition. Accordingly, Figure 1 shows the likelihood  $P(\tau_{2C}|I_2)$  increasing along the diagonal  $t_x = t_y$ . However, for a topology to be deemed  $\tau_{1C}$  by the root shape condition, one of the clades must be ancestral. Figure 1 shows that this pulls  $P(\tau_{1C}|I_2)$  back to a lower region near the origin, where the evolutionary separation condition is less likely to be satisfied. This reflects a straightforward reality; to produce two clades of similar sizes, separated by two or more mutations, with one of the clades being ancestral, requires a relatively unusual accident of growth or evolution. Where the authors omitted the relative size and evolutionary separation conditions, and replaced the root shape condition with the marginalization, they bypassed this conflict.

I then calculated Bayes factors using Equation 2, the new likelihoods, the

authors' posterior probabilities and the compatibility equations 6 and 7. The resulting Bayes factors are shown in Figure 2.

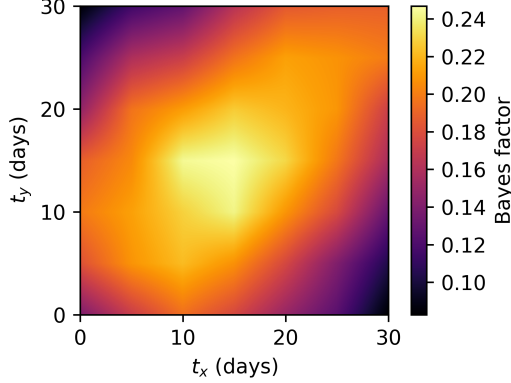


Figure 2: Bayes factors for introduction timings  $(t_x, t_y)$

Notably, Figure 2 shows a maximum Bayes factor at  $t_x = t_y = 15$  days, close to the timings for the maximum likelihood  $P(\tau_{1C}|I_2)$  shown in Figure 1. This reflects the fact that the topology  $\tau_{1C}$  is compatible with the more credible ancestral haplotype  $S_A$ , so the likelihood  $P(\tau_{1C}|I_2)$  is given greater weight in the Bayes factor. The maximum Bayes factor was 2.47. The surface is also fairly flat, suggesting that a model or marginalization of  $(t_x, t_y)$  should produce a Bayes factor around 0.2.

Additionally, the likelihood  $P(\tau_{2C}|I_2)$  does not have a maximum inside the observed range. In order to check for a higher Bayes factor elsewhere, I calculated Bayes factors with the likelihood  $P(\tau_{2C}|I_2)$  maximized at  $(t_x, t_y) = (\infty, \infty)$  and the likelihood  $P(\tau_{1C}|I_2)$  taken from  $(t_x, t_y) = (30, 30)$ , as an upper bound. The result ( $BF = 0.205$ ) indicates that  $P(\tau_{2C}|I_2)$  cannot cause a higher Bayes factor elsewhere. This reflects the lower weight the Bayes factor gives to  $P(\tau_{2C}|I_2)$  for being compatible with the less credible ancestral haplotypes  $S_C, S_T$ .

Incidentally, if the two clades are not required to arise from the two introductions, the Bayes factor is trivially maximized at  $(t_x, t_y) = (0, 0)$ , i.e. simultaneous introduction of identical viruses, so that the combined behavior is similar to a single introduction. However, this is not relevant to the hypothesis that the two clades arose from separate introduction.

The results using the modelled diversity are compared to the authors' reported results in Table 1. The one-introduction likelihoods are reproduced accurately. The two-introduction likelihoods are reduced by an order of magnitude. The Bayes factor is reduced to 0.3, reversing direction to indicate at least moderate support against the report's conclusions.

	As reported	Re-analysis with modelled diversity
Failure rate	77.8%	78.4%
$P(\tau_{1C} I_1)$	3.1%	3.1%
$P(\tau_{2C} I_1)$	0.0%	0.1%
$P(\tau_{1C} I_2)$	11.3%*	0.5%**
$P(\tau_{2C} I_2)$	11.3%*	1.6%**
BF	4.3	<0.3

\* equivalent portion of  $P((\tau_P, \tau_P)|I_2)$

\*\* at  $(t_x, t_y) = (15, 15)$  days, for max. BF

Table 1: Comparison of results as reported and from re-analysis with modelled diversity.

## Evaluating the effect with implicit diversity

If it is assumed that the influence of the molecular clock is negligible, conflict between conditions is bypassed. A more structured diversity might be assumed. For the purposes of replication, I used the same implicit upstream diversity that the authors used in their analysis, but added the relative size condition.

Since the root shape condition is obviated, the two-introduction topology is  $(\tau_P, \tau_P)$ .

In order to maximise the likelihood of the two introductions satisfying the relative size condition, I assumed the introductions were simultaneous.

In order to estimate the two-introduction likelihood, I applied the authors' mutation simulation and clade analysis protocol to 110,000 virus trees from combined simulations that had simultaneous introduction times. I simulated evolution from the clade root following each introduction. I did not consider evolution upstream of the clade roots because it is irrelevant to  $(\tau_P, \tau_P)$ . I then tested the two clades against the relative size condition and for basal polytomies, to count the proportion of virus trees with topologies  $(\tau_P, \tau_P)$ . The resulting two-introduction likelihood was  $P((\tau_P, \tau_P)|I_2) = 2.5\%$ .

I then calculated a Bayes factor using Equation 2, the new likelihoods, the authors' posterior probabilities, and the compatibility equations 5, 6, and 7. The results are compared to the authors' reported results in Table 2. The two-introduction likelihood is reduced by an order of magnitude. The Bayes factor is reduced to below 0.5, reversing direction against the report's conclusions.

With this approach the Bayes factor is approximately twice that estimated using the modelled diversity.

The diversity in this approach arises from the broad compatibility assigned to  $(\tau_P, \tau_P)$  and the authors' prior assumption that all ancestral haplotypes are equally probable. These make  $(\tau_P, \tau_P)$  equally compatible with each of the ancestral haplotypes  $S_A$ ,  $S_B$ ,  $S_C$  and  $S_T$ , and it is weighted accordingly in the Bayes factor calculation. This implies that the introduced diversity must lead to diversity at the clade roots equivalent to 50%  $\tau_{1C}$  and 50%  $\tau_{2C}$ . However,

	As reported	Re-analysis with implicit diversity
Failure rate	77.8%	78.4%
$P(\tau_{1C} I_1)$	3.1%	3.1%
$P(\tau_{2C} I_1)$	0.0%	0.1%
$P((\tau_p, \tau_p) I_2)$	22.6%	2.5%
BF	4.3	0.5

Table 2: Comparison of results as reported and from re-analysis with the authors’ implicit diversity.

approximately 35% of simulated introductions gain a mutation before they found a clade. This implies that the introduced diversity must have a higher proportion of  $\tau_{1C}$ , since a portion of ancestral haplotypes would gain mutations before the clade root, causing introduced  $\tau_{1C}$  shapes to evolve to  $\tau_{2C}$ .

Thus the approach used here, and by the authors, implicitly assumes upstream diversity that causes:

- a 100% probability of a two-mutation separation between introductions;
- a greater than 50% probability of introducing ancestor-descendent pairs.

The Bayes factor should be interpreted in view of this assumption.

## Summary

The authors imposed three additional conditions on the one-introduction model. Two were simple constraints. The other determined weighting.

When one of the constraints was applied to the two-introduction model, the Bayes factor was reduced from 4.3 to 0.5. In this case upstream diversity was not modelled. Instead, as in the authors’ analysis, it arose implicitly from compatibility statements and an assumption that ancestral haplotypes had equal probabilities, which indirectly implied that all introduced pairs were separated by two or more mutations, and that more than 50% were ancestor-descendant pairs.

When the authors’ implicit upstream diversity was replaced by a tuned model, so that all three additional conditions could be applied to the two-introduction model, the Bayes factor was further reduced to 0.3.

No corrections were made for the additional free parameters and beneficial assumptions afforded to the two-introduction model.

When the conditions applied to the two-introduction model are made consistent with those that the authors applied to the one-introduction model, the Bayes factor is reduced by an order of magnitude, and the previously reported quantitative support is reversed. The credibility of the multiple introduction hypothesis should be re-examined in light of this reversal.



## Methods

*Simulation of epidemics* followed the authors’ protocol. For each attempted introduction, a contact network of 5 million nodes was generated with the Barabási–Albert algorithm [3], starting from 8 unconnected nodes, adding 8 edges with each new node, using preferential attachment and retrying self- and duplicate-edges. Disease progression was modelled using seven states: susceptible ( $S$ ); exposed ( $E$ ); pre-symptomatic and infectious ( $P$ ); symptomatic, infectious and unascertained ( $U$ ); symptomatic, infectious and ascertained ( $A_1$ ); symptomatic, infectious, ascertained and proceeding to hospitalization ( $A_2$ ); hospitalized ( $H$ ); and recovered ( $R$ ). The standard disease progression was

$$S \rightarrow E \rightarrow P \rightarrow U \rightarrow R.$$

However, a fraction of cases became ascertained, progressing as

$$S \rightarrow E \rightarrow P \rightarrow A_1 \rightarrow R.$$

A fraction of ascertained cases also became hospitalised, progressing as

$$S \rightarrow E \rightarrow P \rightarrow A_1 \rightarrow A_2 \rightarrow H \rightarrow R.$$

Nodes in the infectious states  $P$ ,  $U$ ,  $A_1$  and  $A_2$  transmitted to neighbouring nodes in the susceptible  $S$  state. The transmission rate for the pre-symptomatic and unascertained states  $P$  and  $U$  was a fraction of that for the ascertained states  $A_1$  and  $A_2$ . All processes were modelled as Poisson. Parameters for the epidemic simulations, and their sources, are in Table 3.

When a susceptible node became exposed with more than one infectious neighbour, a single source was randomly selected from among the infectious neighbours, with odds weighted according to transmission rates.

Each attempted introduction was started by initializing a single randomly selected node in the exposed  $E$  state, with the rest susceptible  $S$ , and run for 100 days. An introduction was deemed successful if, at the end of the simulation, at least 400 infections had occurred and at least one infection was not recovered. Additionally, I always deemed an introduction successful if it reached 50,000 infections (I considered the likelihood of the epidemic dying out within the 100 days after reaching 50,000 infections to be negligible). I repeatedly attempted introductions to generate epidemics for 110,000 successful introductions.

Each successful simulated epidemic produced a transmission network, detailing the progression of the epidemic across the network, and a list of disease events, detailing the progression of the disease in each infected host.

Notably, although the simulations followed the protocol described by the authors, they differed from what was actually implemented by the authors. The authors hard coded their script to ignore commands to initialize the primary case in the exposed state ( $E$ ) and instead initialized the primary case in the pre-symptomatic and infectious state ( $P$ ). I assumed the protocol and command indicated the intended behaviour and therefore initialized the primary case in the exposed state ( $E$ ).

Parameter	Value	Source
Mean number of contacts	16	[4]
Mean duration in $E$	2.9 days	[5], [6]
Mean duration in $P$	2.3 days	[5], [6]
Mean duration in $U$	2.9 days	[7]
Mean duration in $A_1$	2.9 days	[7]
Mean duration in $A_2$	8.1 days	[8]
Mean duration in $H$	30 days	[7]
Fraction ascertained	0.15	[7]
Fraction of ascertained hospitalized	0.5	[1]
Transmission rate of ascertained	0.0175 /contact/day	[1]
Ratio of transmission rate for unascertained over ascertained	0.55	[9]

Table 3: Parameters for the epidemic simulations.

*Combining epidemics* did not follow the authors’ protocol. The authors merely assumed that each introduction was independent, and calculated  $P((\tau_p, \tau_p)|I_2)$  as  $P(\tau_p|I_1)^2$ . Instead, I drew from the 110,000 successful epidemics, with replacement, to obtain 110,000 pairs of successful epidemics  $(E_x, E_y)$ . For each pair of introductions, I made 49 unique combinations with timings from  $(t_x, t_y) \in \{0, 5, 10, 15, 20, 25, 30\}^2$ .

For each combined transmission network, I added an MRCA that immediately divided into two lineages, and made the two lineages transmit to the primary cases of the epidemics  $E_x$  and  $E_y$  at  $t_x$  and  $t_y$ , respectively. I also offset the timings of the transmissions in  $E_x$  and  $E_y$  by  $t_x$  and  $t_y$ , respectively, and merged them into the combined transmission network. I stopped the merge once 50,000 transmissions had been included, or once one of the two simulations had reached its end time - whichever came first.

For each combined list of disease events, I offset the timings of the disease events in  $E_x$  and  $E_y$  by  $t_x$  and  $t_y$ , respectively, and merged them into a combined disease events list. I only included disease events for cases included in the combined transmission network, and I stopped the merge once one of the two simulations had reached its end time.

*Simulation of sequencing* followed the authors’ protocol. For each ascertained case among the first 50,000 infections of an epidemic or combined epidemic, a notional sequence was sampled at a time randomly selected from a period starting from symptom onset (i.e.  $P \rightarrow A_1$ ) and ending at recovery (i.e.  $A_1 \rightarrow R$  or  $H \rightarrow R$ ). Sequences with sampling times preceding the first hospitalization (i.e. the first  $A_2 \rightarrow H$ ) were discarded. If the start of the period for a hospitalized case preceded the first hospitalization, it was set to the time of the first hospitalization, in order to ensure that all hospitalized cases were sequenced. If an ascertained case had not recovered by the end of the simulation, the end of the period was set to the end of the simulation.

*Simulation of coalescence* followed the authors’ protocol. For each epidemic and combined epidemic, the ancestry of the simulated virus samples was traced back through the transmission network to produce a virus phylogeny. Within hosts, lineages were merged with Kingman’s coalescent under a fixed effective population of one year. For events between a host’s earliest transmission and infection, the exponential distribution used to sample waiting times was truncated, in order to ensure a single lineage at the time of infection.

*Simulation of evolution* followed the authors’ protocol. Mutations were approximated as unique and irreversible, and simulated along the virus phylogeny as a Poisson process, at a rate of one mutation every 13.27 days.

*Clade analysis* followed the authors’ protocol. Lineage numbers included all leaves and mutated internal nodes descending directly from a clade root (i.e. without intermediate mutated nodes). Clade sizes counted all leaves descending directly or indirectly from clade roots.

*Checking if two clades arose from two introductions* was performed by running the clade analysis for two-introduction trees with the clade roots manually set to the first internal nodes following each introduction.

*Stable coalescence* was not used. The stable coalescence effectively prunes short-lived basal lineages. Therefore, it might increase the one-introduction likelihoods, but should have no effect on the two-introduction likelihoods, because the basal lineages of the two introductions always succeed, as a condition of Equation 1. However, the authors did not explain the reason for using the stable coalescence. Therefore, I concluded that using the stable coalescent could only benefit the one-introduction case, without reason, and decided to omit it. The one-introduction likelihoods nonetheless almost perfectly matched those of the authors, suggesting that the effect of the stable coalescence is less than the sampling error, and that the effect of the omission was negligible.

## Data and reproducibility

Results and code are available at <https://github.com/nizzaneela/re-multi-introductions>.

The results include the clade analysis result for each simulated virus tree along with a hash of the corresponding tree.

The code includes a script for reproducing all simulations and a notebook for collating the results. A separate notebook provides verification of the clade analysis results and hashes from arbitrary simulations.

The scripts simulate the epidemics using a modified version of Futing Fan’s implementation [10] of GEMF [11] [12], available at <https://github.com/nizzaneela/GEMF>. The modified version of GEMF includes Niema Moshiri’s modifications to read a seed for the pseudo-random number generator from the input file.

The scripts use CoaTran [13] for coalescence and TreeSwift [14] for the clade analysis.

## References

- [1] Jonathan E. Pekar, Andrew Magee, Edyth Parker, Niema Moshiri, Katherine Izhikevich, Jennifer L. Havens, Karthik Gangavarapu, Lorena Mariana Malpica Serrano, Alexander Crits-Christoph, Nathaniel L. Matteson, Mark Zeller, Joshua I. Levy, Jade C. Wang, Scott Hughes, Jungmin Lee, Heedo Park, Man-Seong Park, Katherine Ching Zi Yan, Raymond Tzer Pin Lin, Mohd Noor Mat Isa, Yusuf Muhammad Noor, Tetyana I. Vasylyeva, Robert F. Garry, Edward C. Holmes, Andrew Rambaut, Marc A. Suchard, Kristian G. Andersen, Michael Worobey, and Joel O. Wertheim. The molecular epidemiology of multiple zoonotic origins of sars-cov-2. *Science*, 377(6609):960–966, 2022.
- [2] Erratum for the research article “The molecular epidemiology of multiple zoonotic origins of SARS-CoV-2” by J. E. Pekar *et al.* *Science*, 382(6667):eadl0585, 2023.
- [3] Albert-László Barabási and Réka Albert. Emergence of scaling in random networks. *science*, 286(5439):509–512, 1999.
- [4] Joël Mossong, Niel Hens, Mark Jit, Philippe Beutels, Kari Auranen, Rafael Mikolajczyk, Marco Massari, Stefania Salmaso, Gianpaolo Scalia Tomba, Jacco Wallinga, et al. Social contacts and mixing patterns relevant to the spread of infectious diseases. *PLoS medicine*, 5(3):e74, 2008.
- [5] Xi He, Eric HY Lau, Peng Wu, Xilong Deng, Jian Wang, Xinxin Hao, Yiu Chung Lau, Jessica Y Wong, Yujuan Guan, Xinghua Tan, et al. Temporal dynamics in viral shedding and transmissibility of covid-19. *Nature medicine*, 26(5):672–675, 2020.
- [6] Qun Li, Xuhua Guan, Peng Wu, Xiaoye Wang, Lei Zhou, Yeqing Tong, Ruiqi Ren, Kathy SM Leung, Eric HY Lau, Jessica Y Wong, et al. Early transmission dynamics in wuhan, china, of novel coronavirus–infected pneumonia. *New England journal of medicine*, 382(13):1199–1207, 2020.
- [7] Xingjie Hao, Shanshan Cheng, Degang Wu, Tangchun Wu, Xihong Lin, and Chaolong Wang. Reconstruction of the full transmission dynamics of covid-19 in wuhan. *Nature*, 584(7821):420–424, 2020.
- [8] An Pan, Li Liu, Chaolong Wang, Huan Guo, Xingjie Hao, Qi Wang, Jiao Huang, Na He, Hongjie Yu, Xihong Lin, et al. Association of public health interventions with the epidemiology of the covid-19 outbreak in wuhan, china. *Jama*, 323(19):1915–1923, 2020.
- [9] Ruiyun Li, Sen Pei, Bin Chen, Yimeng Song, Tao Zhang, Wan Yang, and Jeffrey Shaman. Substantial undocumented infection facilitates the rapid dissemination of novel coronavirus (sars-cov-2). *Science*, 368(6490):489–493, 2020.

- [10] Futing Fang. Improving GEMFsim: a stochastic simulator for the generalized epidemic modeling framework. Master of Science Thesis, Kansas State University, Manhattan, KS, USA, December 2019. Major Professor: Caterina M. Scoglio.
- [11] Faryad Darabi Sahneh, Caterina Scoglio, and Piet Van Mieghem. Generalized epidemic mean-field model for spreading processes over multilayer complex networks. *IEEE/ACM Transactions on Networking*, 21(5):1609–1620, 2013.
- [12] Faryad Darabi Sahneh, Aram Vajdi, Heman Shakeri, Futing Fan, and Caterina Scoglio. Gemfsim: A stochastic simulator for the generalized epidemic modeling framework. *Journal of Computational Science*, 22:36–44, 2017.
- [13] Niema Moshiri. Coatran: Coalescent tree simulation along a transmission network. *bioRxiv*, 2020.
- [14] Niema Moshiri. Treeswift: A massively scalable python tree package. *SoftwareX*, 11:100436, 2020.